Calcium Currents in Hair Cells Isolated from Semicircular Canals of the Frog

M. Martini, M. L. Rossi, G. Rubbini, and G. Rispoli
Istituto Nazionale per la Fisica della Materia, Dipartimento di Biologia dell'Università-Sezione di Fisiologia Generale, 44100 Ferrara, Italy

ABSTRACT L-type and R-type Ca^{2+} currents were detected in frog semicircular canal hair cells. The former was noninactivating and nifedipine-sensitive (5 μM); the latter, partially inactivated, was resistant to ω-conotoxin GVIA (5 μM), ω-conotoxin MVIIC (5 μM), and ω-agatoxin IVA (0.4 μM), but was sensitive to mibefradil (10 μM). Both currents were sensitive to Ni^{2+} and Cd^{2+} (>10 μM). In some cells the L-type current amplitude increased almost twofold upon repetitive stimulation, whereas the R-type current remained unaffected. Eventually, run-down occurred for both currents, but was prevented by the protease inhibitor calpastatin. The R-type current peak component ran down first, without changing its plateau, suggesting that two channel types generate the R-type current. This peak component appeared at −40 mV, reached a maximal value at −30 mV, and became undetectable for voltages ≥0 mV, suggestive of a novel transient current: its inactivation was indeed reversibly removed when Ba^{2+} was the charge carrier. The L-type current and the R-type current plateau were appreciable at −60 mV and peaked at −20 mV: the former current did not reverse for voltages up to +60 mV, the latter reversed between +30 and +60 mV due to an outward Cs^{+} current flowing through the same Ca^{2+} channel. The physiological role of these currents on hair cell function is discussed.

INTRODUCTION

In hair cell function, K^{+} and Ca^{2+} ions play an essential role. Indeed, K^{+} carries the transduction current at the apical ciliated pole of the cell, where localized changes in cytosolic Ca^{2+} concentration, $[Ca^{2+}]_i$, modulate the transduction process (Hudspeth and Gillespie, 1994) and regulate receptor potential amplitude. The receptor potential, in turn, activates basolateral Ca^{2+} and K^{+} conductances, which ultimately control transmitter release at the cytoneural junction. Voltage-dependent K^{+} and Ca^{2+} currents have been studied in hair cells belonging to organs specialized in detecting either acoustic stimuli or vibratory and angular accelerations. However, in semicircular canal hair cells, greater attention has been devoted to defining the properties of the K^{+} rather than the Ca^{2+} channels (Ohmori, 1984; Hudspeth and Lewis, 1988; Housley et al., 1989; Lang and Correia, 1989; Fuchs and Evans, 1990; Fuchs et al., 1990; Rennie and Ashmore, 1991; Norris et al., 1992; Masetto et al., 1994; Zidanic and Fuchs, 1995; Steinacker et al., 1997). Moreover, most of these studies have been carried out on enzymatically dissociated cells. Ampullar receptors selectively transduce the angular acceleration of the head into phasic and tonic afferent nerve fiber firing patterns, and these functions are regulated by specific changes in basolateral conductances. Rossi et al. (1994) have demonstrated that, in the intact labyrinth isolated from the frog head, the Ca^{2+} influx into posterior canal hair cells is essential in modulating the rate of the asynchronous, uncorrelated quantal transmitter release at the afferent synapse. Indeed, the increase (decrease) in spontaneous mEPSP rate in high (low) extracellular Ca^{2+}, $[Ca^{2+}]_o$, is related to the increase (decrease) in inward Ca^{2+} current. The existence of distinct types of voltage-dependent Ca^{2+} channels in different preparations has been demonstrated through kinetic studies, pharmacological treatments, and molecular cloning (see reviews by McCleskey, 1994; Dunlap et al., 1995).

The properties of the Ca^{2+} channels in semicircular canal hair cells, however, are less known; in the acoustic-vestibular system, pharmacological studies have indicated the existence of a single population of L-type Ca^{2+} channels. However, the voltage activation threshold of these channels was more negative than observed in neuronal L-type channels (Lang and Correia, 1989; Zidanic and Fuchs, 1995). In the semicircular canal, homogeneous populations of L-type and T-type channels have been identified in the frog (Prigioni et al., 1992) and in the guinea-pig, respectively (Rennie and Ashmore, 1991). Nonetheless, other studies suggested the existence of additional channel types (Su et al., 1995; Green et al., 1996; Perin et al., 1998) in these preparations. Given the relevance of Ca^{2+} in controlling both the transduction process and transmitter release, and given the poor and rather conflicting information about canal hair cell Ca^{2+} channels, the present work is focused on the properties of Ca^{2+} currents in hair cells mechanically isolated from frog semicircular canals.

Received for publication 10 May 1999 and in final form 3 December 1999.

Address reprint requests to Dr. Giorgio Rispoli, Dipartimento di Biologia dell'Università-Sezione di Fisiologia Generale, Via Borsari 46, 44100 Ferrara, Italy. Tel.: 39-0532-291473/291462; Fax: 39-0532-207143; E-mail: rsg@dns.unife.it.

© 2000 by the Biophysical Society

0006-3495/00/03/1240/15 $2.00

METHODS

Dissociation of hair cells

The experiments were performed on wild frogs (*Rana esculenta*, 25–30 g body weight) that were mainly harvested in summer. The animals were anesthetized by immersion in tricaine methane sulfonate solution (1 g/l in water) and subsequently decapitated. The heads were pinned down at the

bottom of the dissection chamber and submerged in a dissection solution of the following composition (in mM): 120 NaCl, 2.5 KCl, 0.5 EGTA, 5 HEPES, 20 sucrose, 3 glucose (pH 7.2). The osmolality of the solution (260 mOsmol/kg) was measured with a microosmometer (Hermann Roebling, Messtechnik, Berlin, Germany). The six ampullae were isolated from both labyrinths and transferred into the experimental chamber (500 μl volume). The hair cells were mechanically dissociated from the ampullae by gently scraping the epithelium with fine forceps. The experimental chamber had Teflon walls and a bottom consisting of a glass microscope coverslip coated with chloro-tri-*n*-butyl-silane to prevent cell sticking.

Pipette and recording solutions

Electrical recordings were carried out by using the patch-clamp recording technique in the "whole-cell" configuration. Pipettes were pulled in the conventional manner (Hamill et al., 1981) from 50 μl glass capillaries (Drummond, Broomall, PA), and fire-polished to a pipette resistance of 3–4 MΩ. Pipette solutions consisted of the following common components (in mM): 90 CsCl, 20 tetraethylammonium chloride (TEACl), 2 $MgCl_2$, 1 adenosine 5′-triphosphate K^+ salt (ATP), 0.1 guanosine 5′-triphophate Na^+ salt (GTP), 10 HEPES (pH 7.2, 235 mOsmol/kg). Three different concentrations of EGTA and Ca^{2+} were added to this base solution. One solution was Ca^{2+}-free and contained 5 mM EGTA, another was EGTA-free and contained 0.5 mM Ca^{2+}, and a third solution contained 10 μM EGTA + 10 μM Ca^{2+}. In some recordings, Cs^+ was substituted with an equiosmolar concentration of *N*-methyl-glucamine (NMG^+); the membrane potential of these recordings was corrected for the junction potential (9 mV; Block and Jones, 1997) with respect to Cs^+. When used, calpastatin was dissolved in the pipette solution (2 U/ml) and purified by overnight dialysis at 4°C in a large volume (2.5 l) of a calpastatin-free solution (the membrane used allowed the diffusion of all molecules with a molecular weight <10 kDa). To facilitate the formation of the gigaseal in the calpastatin experiments, the calpastatin solution was used to backfill the electrode, whereas the pipette tip was filled with a calpastatin-free solution. The composition of the chamber solution was (in mM): 100 NaCl, 6 CsCl, 20 TEACl, 4 $CaCl_2$, 10 HEPES, 6 glucose (pH 7.2, 260 mOsmol/kg). The channel antagonists were used at the following concentrations: 10, 300, and 1000 μM Ni^{2+}; 10 and 200 μM Cd^{2+}; 2 and 10 μM mibefradil; 1, 5, and 10 μM ω-conotoxin GVIA; 1, 5, and 10 μM nifedipine; 5 μM ω-conotoxin MVIIC; 0.2 and 0.4 μM ω-agatoxin IVA. All drugs were dissolved in water, except nifedipine, which was dissolved in dimethyl sulfoxide. All channel antagonist solutions were prepared on the day of the experiments, by dissolving the powder (or an aliquot from a stock solution stored at −20°C for Ni^{2+}, Cd^{2+}, and nifedipine) directly into the perfusion system bottles. The external solution was changed rapidly (typically <50 ms) by horizontally moving (with a computer-controlled stepping motor) a multibarrelled perfusion pipette placed in front of the recorded cell. The perfusion solution was removed by a peristaltic pump (Masterflex, Cole-Parmer, Vernon, IL), which also constantly circulated the solution within the recording chamber. All experiments were performed at room temperature (20–22°C). All salts, buffers, and solvents were purchased from Sigma Chemical Co. (St. Louis, MO); nifedipine and ω-conotoxin MVIIC from Alomone Labs (Jerusalem, Israel); ω-conotoxin GVIA from Bachem Feinchemikalien AG (Bubendorf, Switzerland) and from Alomone Labs; ω-agatoxin IVA from Calbiochem (La Jolla, CA); mibefradil was a generous gift from F. Hoffmann-La Roche (Basel, Switzerland).

Cell viewing

Cells were viewed through a TV monitor (Sony, Tokyo, Japan) connected to a contrast enhanced video camera (T.I.L.L. Photonics, Planegg, Germany). The camera was coupled to an inverted microscope (Olympus IMT-2, Tokyo, Japan) equipped with a 40× Hoffman modulation contrast objective. Cell video images were recorded at the beginning and at the end of each experiment with a commercial VCR (Panasonic NV-HS1000EGC, Matsushita Electric Industrial Co., Ltd., Osaka, Japan) and digitized off-line by an AV-Master computer interface (Fast Multimedia, Münich, Germany) hosted in a Pentium IBM-compatible computer.

Patch-clamp recording and data analysis

The current was recorded with a commercial patch-clamp amplifier (EPC-7, List-Electronic, Darmstadt, Germany); the holding potential was −70 mV, unless otherwise specified. In all recordings, Ca^{2+} currents were elicited after measuring the leak resistance with a 15-ms hyperpolarization to −80 mV from the holding potential. The seal resistance ranged between 5 and 50 GΩ, the access resistance between 15 and 25 MΩ, and the input resistance between 1 and 5 GΩ. The pipette and cell capacitances were compensated using the corresponding EPC-7 controls; access resistance was compensated up to 50–70%. Cell capacitance ranged between 4 and 12 pF (7.1 ± 0.3 pF; 53 cells) and was not apparently correlated with cell morphology (Fig. 1). Perfect cancellation of the RC artifacts was rarely attained during the recordings, and the traces were corrected off-line using several different procedures. If the artifacts were particularly small and/or significantly faster than the activation and deactivation kinetics, then their

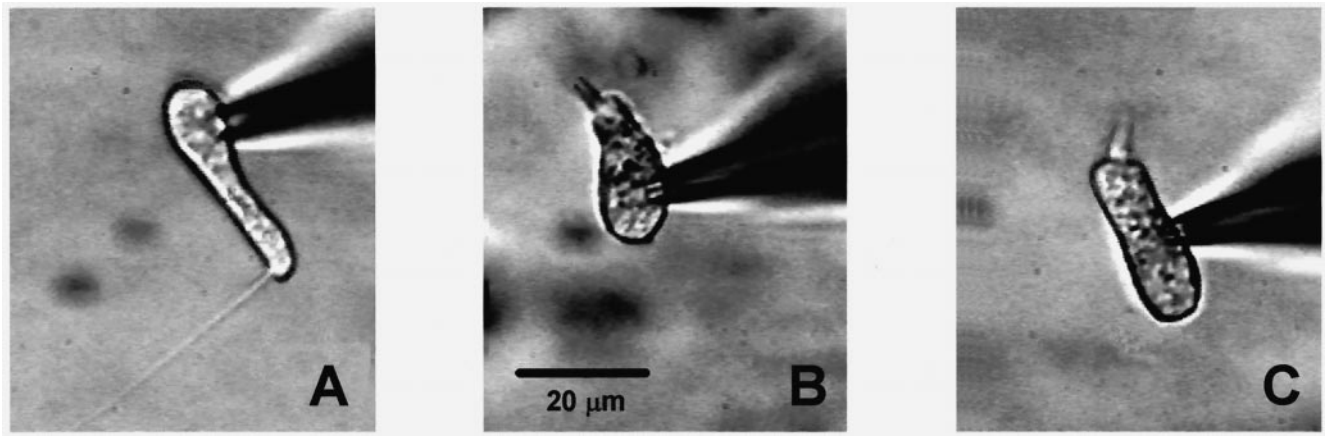

FIGURE 1 Video recordings, at the end of a whole-cell experiment, of (A) a club-like, (*B*) a pear-like, and (*C*) a cylinder-like hair cell.

digital points were removed. Large and/or slow artifacts were recorded either at the end of run-down (when no Ca^{2+} current was present; see Results) or in the presence of 200 μM Cd^{2+} (when all the Ca^{2+} channels are blocked). The artifacts were then subtracted from the uncorrected Ca^{2+} current waveforms. These subtraction procedures gave very similar results. The command protocol and data acquisition were performed with a Labmaster computer interface and a pClamp package (Version 6.0.3, Axon Instruments, Foster City, CA) running on a Pentium IBM-compatible computer. The recordings, filtered at 2, 6, or 10 kHz via an eight-pole Butterworth filter (LPBS-48DG, NPI Electronic, Tamm, Germany), were acquired at 5, 12.5, or 40 kHz, respectively, and stored on disk. The data were also digitized in PCM format and stored on DAT tapes by using a digital recorder (DTR-1802, Biologic, Claix, France, bandwidth 0–20 kHz). The figures were prepared by using a commercial plotting program (Version 3.0, Sigmaplot, Jandel Scientific, San Rafael, CA) and a picture editor (Corel Draw, Ottawa, Ontario, Canada). All mathematical procedures (data fitting and equation solving) were implemented with Mathcad (Version 7.0, Mathsoft, Bagshot, Surrey, UK). The values in text and figures are given as means ± SE throughout the paper.

RESULTS

Ca^{2+} current waveform

In most cells a depolarization was able to elicit an inward current when Cs^+ and TEA^+ were present in the recording solutions. Typically, cells that did not exhibit any inward current had an input resistance >3 GΩ and an ohmic I-V relationship, indicating that the experimental conditions were sufficient to block all non-Ca^{2+} endogenous channels. The inward current was assessed by stepping the voltage to −20 mV (Fig. 2). The current amplitude and waveform did

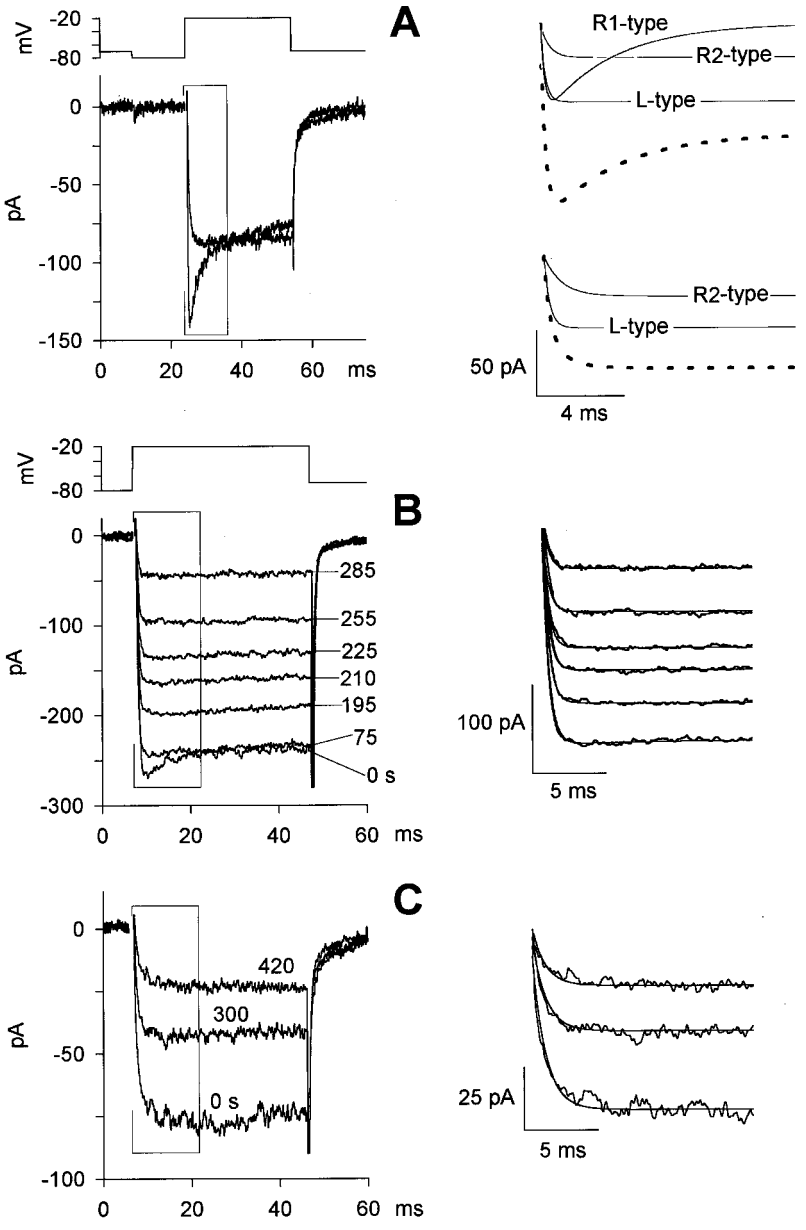

FIGURE 2 Ca^{2+} current waveforms and typical run-down experiments. (*A*) After measuring the leak resistance with a 15-ms hyperpolarization to −80 mV from the holding potential (−70 mV), the Ca^{2+} current was elicited by a 30-ms depolarization to −20 mV. *Left*, typical Ca^{2+} current waveform recorded from two cells, one displaying the sag component and the other lacking it. *Right*, activation and inactivation kinetics of the responses on the left are fitted by Eq. 1 (*dotted traces*). The *solid thin traces* are the contribution of the two R-type and the L-type currents to the total current. The *R1-type* trace was constructed by fitting the sag component, which was singled out (*gray trace*) as discussed in the text. (*B*) Ca^{2+} current run-down in response to repetitive 40-ms depolarizations to −20 mV from a potential of −80 mV, repeated every 15 s; representative traces are shown at seven recording times (indicated in s near each trace). (*C*) Ca^{2+} current run-down in response to the same depolarizing test pulses delivered only at the indicated times (in s above each trace). The fit of representative traces of *B* and *C* to Eq. 1 are superimposed on the data and shown on the right.

not change if the voltage was stepped from any value between −140 and −60 mV: this indicates that, at any voltage below −60 mV, all channels were deactivated and steady-state inactivation was removed.

The Ca^{2+} current had two typical waveforms: one (present in ~40% of the cells) was characterized by an initial peak, followed by an exponential decay to a plateau level (current sag component); the other waveform lacked the sag, and the current amplitude was constant throughout the depolarizing step (Fig. 2 *A*). The sag might have been generated by the opening and the subsequent partial inactivation of a single channel population: however, this view does not explain the absence of the sag in some recordings, nor does it explain the lack of correlation between the sag properties (amplitude and time course) and steady-state current amplitude. The presentation of either of the responses in Fig. 2 was not correlated with the cell morphology (Guth et al., 1994; Fig. 1) and, eventually, those cells exhibiting a sag response ended in a plateau. Indeed, in all experiments, the mean current amplitude was not stable upon repeating the stimulation protocol (consisting of 20 depolarizing steps, from the holding potential to −20 mV, lasting 40 ms and repeated every 15 s), but it progressively declined to zero (run-down). The sag component of the current (when present) was lost much earlier than the plateau component (Fig. 2 *B*, traces between 0 and 75 s). Once the former component had completely disappeared, the latter began a progressive decline toward zero. The sag response can be readily explained by assuming that the depolarization opened at least two channel types, both activating exponentially with a time constant of ~0.5 ms (see the statistics below): the first with an inactivating time constant of few ms, the second which did not inactivate.

Inactivation of Ca^{2+} current was Ca^{2+}-dependent

Fig. 3 provides clear-cut evidence that the sag response was generated by a Ca^{2+} channel exhibiting a Ca^{2+}-dependent inactivation. The sag and the plateau amplitudes were reduced, and sag kinetics slowed down, with a decrease in $[Ca^{2+}]_o$ (Fig. 3 *A*); the sag disappeared when $Ca^{2+}{}_o$ was substituted with $Ba^{2+}{}_o$ (Fig. 3 *B*).

Consistent with the notion that a Ca^{2+}-dependent inactivation is removed in Ba^{2+}, the size of the current increase observed upon substituting Ca^{2+} with Ba^{2+} was smaller in those cells that lacked the sag component than in those where the sag was present (compare Fig. 5 *C* and the corresponding inset on the right with Fig. 5 *D* and the inset on the right). The effects of both $[Ca^{2+}]_o$ reduction and Ba^{2+} substitution were fully reversible upon returning to normal $[Ca^{2+}]_o$ (Fig. 3). To determine whether the Ca^{2+}-dependent inactivation was also voltage-dependent, recovery from inactivation was investigated using the standard two-pulse protocol (Fig. 4). Two depolarizing steps to −20 mV were separated by progressively longer interpulses at two different holding potentials (−70 mV and −120 mV). The time interval between each one of the consecutive double-pulse protocols was 7 s, which guaranteed the full recovery of the test current (Fig. 4 *C*).

Analysis of the fractional amplitude versus interpulse duration indicated that recovery from inactivation required times on the order of 100 ms at −120 mV (Fig. 4 *D*) and 300 ms at −70 mV (Fig. 4, *B* and *D*). Such lengthy recovery times are not consistent with the existence of a voltage-sensitive inactivating gate, which should act much faster; however, it is compatible with the speed at which $[Ca^{2+}]_i$ is restored to its physiological level upon returning to the holding potential.

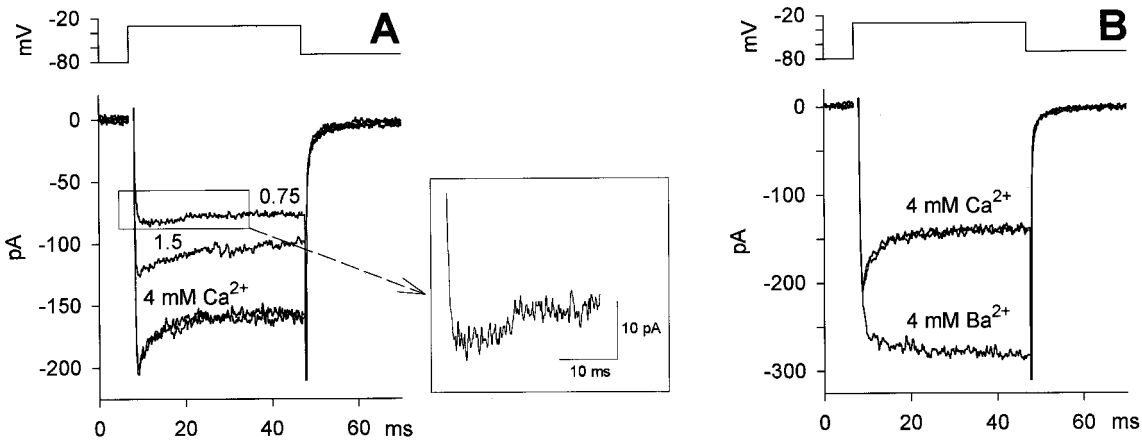

FIGURE 3 Ca^{2+}-dependent inactivation of Ca^{2+} current. Voltage was stepped to −30 mV to maximize the sag component. (*A*) Effect of $[Ca^{2+}]_o$ reduction (from 4 mM to 1.5 or 0.75 mM) on the Ca^{2+} current. *Inset*: enlargement of the current trace recorded in 0.75 mM Ca^{2+}, as indicated in the box. (*B*) Absence of inactivation when $Ca^{2+}{}_o$ is replaced by an equiosmolar concentration of Ba^{2+}. In *A* and *B* the two superimposed traces are the control and recovery in 4 mM $[Ca^{2+}]_o$, before and after the perfusion with 1.5 and 0.75 mM $[Ca^{2+}]_o$ (*A*), or 4 mM $[Ba^{2+}]_o$ (*B*).

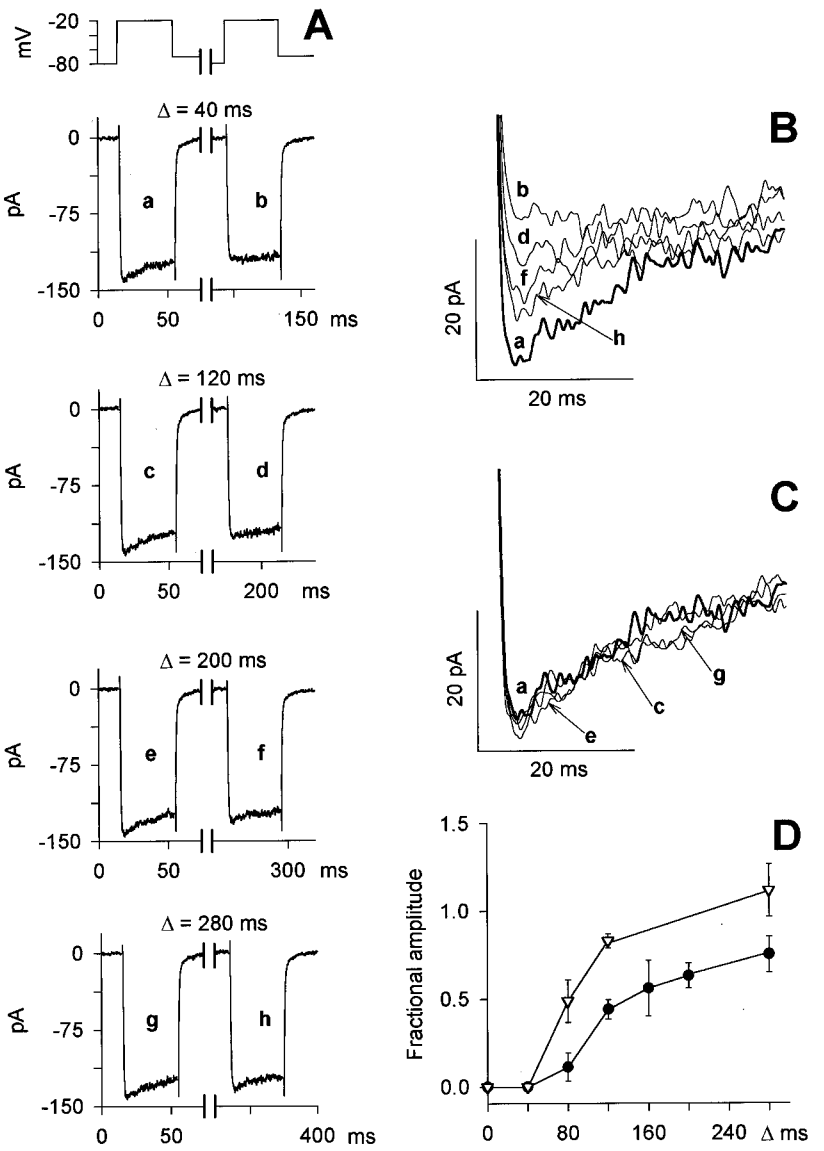

FIGURE 4 Kinetics of current recovery from inactivation. (*A*) After measuring the leak resistance, two consecutive 40-ms depolarizations to −20 mV were delivered, separated by 20, 100, 180, and 260 ms interpulses to −70 mV (interpulse holding potential). All interpulses were followed by an additional 20-ms step to −80 mV to re-evaluate leak resistance before delivering the second pulse (the time Δ is the interpulse duration). The time interval between each of the consecutive double depolarization protocols was 7 s. The Ca^{2+} currents elicited by the first depolarization (*A*, *traces a*, *c*, *e*, and *g*), and by the test depolarization (*A*, *traces b*, *d*, *f*, and *h*) are compared in *C* and *B*, respectively, on a faster time scale; the lowercase letters indicate the same traces in *A*, *B*, and *C*. (*D*) Mean values of the ratio between the peak Ca^{2+} current elicited by the test depolarization and the peak Ca^{2+} current elicited by the prepulse. Interpulse holding potentials were −70 mV (*filled circles*, 8 cells) and −120 mV (*open triangles*, 8 cells).

Ca^{2+} current is generated by an L-type and possibly two R-type channels

In order to identify which channel types generate the Ca^{2+} current waveform, typical Ca^{2+} antagonists were used. It was found that 1 μM nifedipine reduced the current plateau component (leaving the sag component, when present, unaffected) by 57.1 ± 3.6% (n = 5; 5 cells), thus indicating the presence of an L-type channel. Since 5 μM nifedipine reduced the plateau component by 68.4 ± 2.0% (n = 14; 12 cells; Fig. 5), and 10 μM nifedipine produced nearly the same current reduction (again, either concentration did not affect the sag component), it can be concluded that ~70% of the plateau component was carried by an L-type channel. Nifedipine (5 μM) had nearly the same effect on the Ba^{2+} current (reduced by 62.2 ± 3.0%; n = 5; 5 cells; Fig. 5 *D*) when the corresponding current in Ca^{2+} lacked the sag component.

The total current was unaffected by ω-conotoxin GVIA (5 μM; Fig. 6 *A*; 7 cells), ω-conotoxin MVIIC (5 μM; Fig. 6 *B*; 5 cells), and ω-agatoxin IVA (up to 0.4 μM; Fig. 6 *C*; 5 cells), thus ruling out the presence of N- or P/Q-type Ca^{2+} channels. These compounds, as expected, did not affect the nifedipine-resistant current (5 μM nifedipine; Fig. 6 *D*; 4 cells; data shown only for 5 μM ω-conotoxin MVIIC), indicating that this current was flowing through R-type channels.

When present, the sag component remained unaffected by the application of nifedipine, thus indicating that the sag was generated by the inactivation of the R-type current and not by a partial inactivation of the L-type. The progressive loss of the sag component during the initial phase of rundown occurred without any change in the plateau amplitude (Fig. 2 *B*). This fact cannot be accounted for by the progressive loss of a Ca^{2+}-dependent, partial inactivation of a

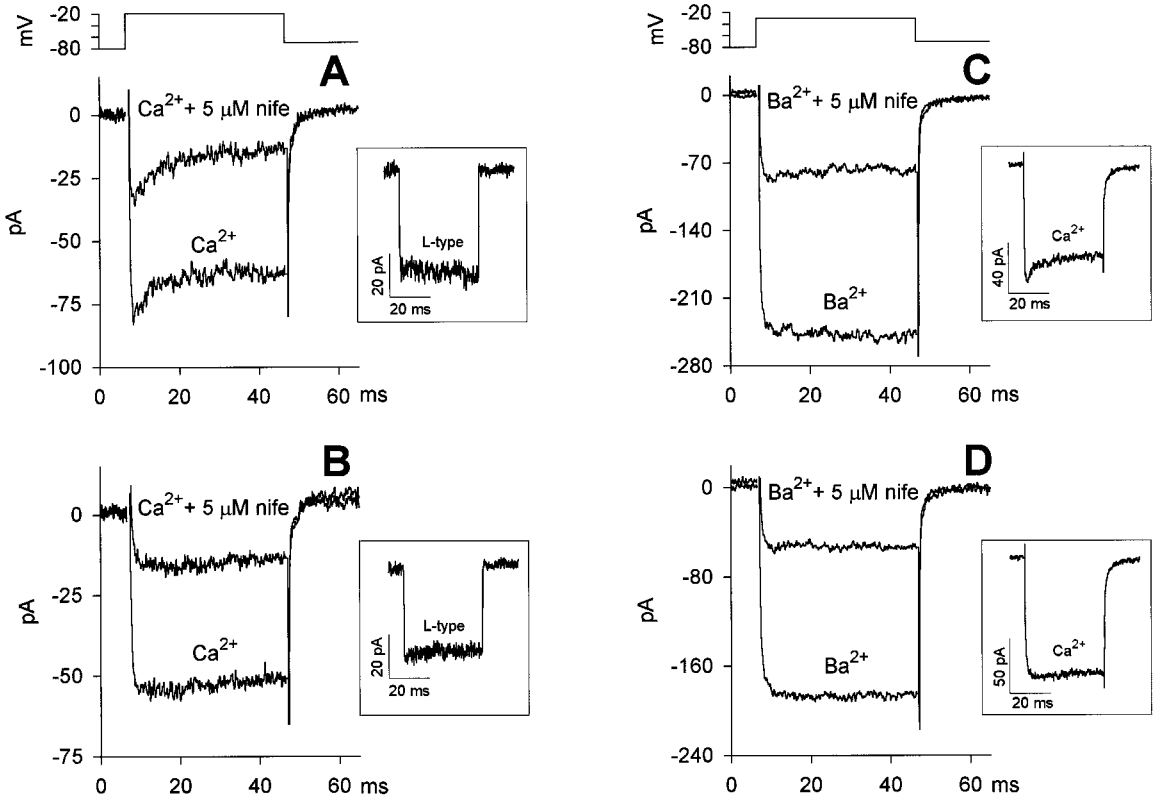

FIGURE 5 Effect of nifedipine on the Ca^{2+} and Ba^{2+} currents (in 4 different cells). The recovery following each nifedipine application was complete and was omitted for clarity. Effect of nifedipine on the Ca^{2+} current in the presence (*A*) and in the absence (*B*) of the sag component; the L-type current resulting from the difference between the two traces on the left in *A* and *B* is shown in the corresponding *inset* on the right. (*C*) Effect of nifedipine on the Ba^{2+} current in a cell presenting the sag component in Ca^{2+} (*inset* on the right) and (*D*) in a cell exhibiting only the plateau component in Ca^{2+} (*inset* on the right).

single R-type channel. Instead, it could be explained by the presence of a third channel type, which runs down completely before the onset of the plateau component reduction. This channel could be a T-type channel: however, no T-type channel has been reported to lose inactivation in Ba^{2+} (Carbone and Lux, 1984; Tsien et al., 1998; Huguenard, 1998). Thus, it can be concluded that two R-type channels generate the current left after the nifedipine application: one generates the sag and fully inactivates in a Ca^{2+}-dependent manner, the other does not inactivate and accounts for the remaining plateau. Besides, both the R-type channels were sensitive to mibefradil, Ni^{2+}, and Cd^{2+}. Indeed, 2 μM mibefradil reduced the sag amplitude by 31 $\pm$ 7% ($n = 3$; 3 cells; data not shown), whereas 10 μM nearly suppressed it (Fig. 7 *A*; 3 cells). Two and 10 μM mibefradil reduced the amplitude of the plateau of the total current by 18 $\pm$ 3% ($n = 9$; 5 cells; data not shown) and by 33 $\pm$ 2% ($n = 3$; 3 cells; Fig. 7 *A*), respectively. This suggests that 10 μM mibefradil abolished both the R-type currents, leaving only the L-type channel to carry the current. Indeed, it has been reported that mibefradil is a potent inhibitor of R-type channels (Randall and Tsien, 1997) and it is more selective for R-type than for L-type channels (Emanuel et al., 1998).

Cd^{2+} and Ni^{2+} were able to block the inactivating R-type channel (Fig. 7, *B* and *C*); however, high concentrations of these cations were able to suppress the total current consistently with the almost complete suppression of the Ba^{2+} current induced by 100 μM Cd^{2+} (Perin et al., 1998). An addition of 10 μM Ni^{2+} was able to suppress the sag currents of small amplitude (data not shown); however, in some experiments this low Ni^{2+} concentration failed to cancel the sag component; rather, it reduced the plateau amplitude, affecting the current waveform in a manner similar to 10 μM Cd^{2+} (Fig. 7 *B*).

In conclusion, the activation-inactivation phase $I_a(t)$ of the Ca^{2+} current waveform can be reasonably described by the following equation (see Figs. 2 and 11):

$$I_a(t) = A_L \cdot (1 - e^{-(t/\tau_{aL})}) + A_{R1} \cdot e^{-(t/\tau_{iR1})} \cdot (1 - e^{-(t/\tau_{aR1})}) + A_{R2} \cdot (1 - e^{-(t/\tau_{aR2})}) \quad (1)$$

where A_L and τ_{aL} are the amplitude and the activation time constant of the L-type current; A_{R1}, τ_{aR1}, and τ_{iR1} are the amplitude, activation, and inactivation time constants of the transient R-type current; A_{R2} and τ_{aR2} are the activation parameters of the plateau R-type current. The responses

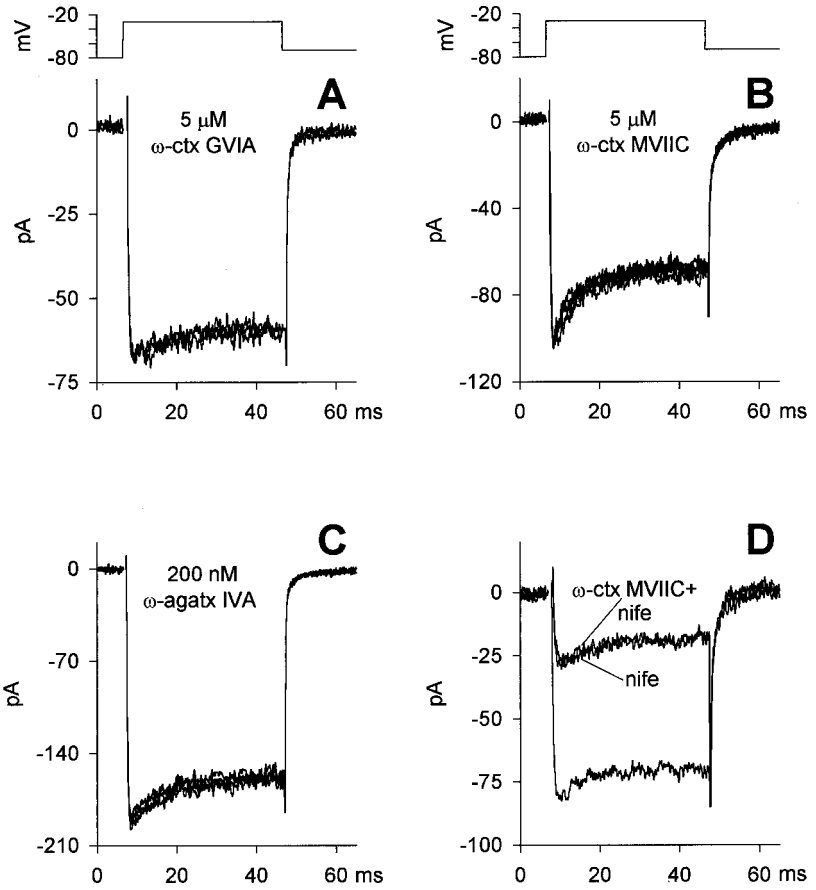

FIGURE 6 Effect of ω-conotoxin GVIA, ω-conotoxin MVIIC, and ω-agatoxin IVA on the peak and the plateau component of the Ca^{2+} current in three representative cells. (*A–C*) The responses to at least three subsequent depolarizing test pulses to −30 mV in the presence of the antagonist (indicated above each trace family) are compared with the control traces recorded before and after antagonist application. The effect of ω-conotoxin MVIIC during the nifedipine application is shown in *D* in a fourth cell.

consisting of only the steady-state component were interpolated by Eq. 1 with $A_{R1} = 0$. The average amplitude of the plateau component, that is $A_L + A_{R2}$, was −126 ± 8 pA (range: −70 to −370 pA; 53 cells); the absolute values of A_L and A_{R2} can be estimated from the relationship $A_L \sim 2.3 \times A_{R2}$, drawn from the nifedipine experiments (Fig. 5). The A_{R1}, τ_{R1}, and τ_{iR1} values were obtained upon fitting the sole experimental sag component. The sag was singled out (Fig. 2 *A*, *right panel*) by subtracting the current recorded after the full run-down of the sag from the total current recorded at the beginning of an experiment (an example is shown in Fig. 2 *B*, traces at 0 and 75 s). The results of this procedure were $\tau_{iR1} = 6.7 \pm 0.8$ ms (range: 3–15 ms; $n = 22$; 22 cells); $A_{R1} = -42 \pm 5$ pA (range: −10 to −95 pA;

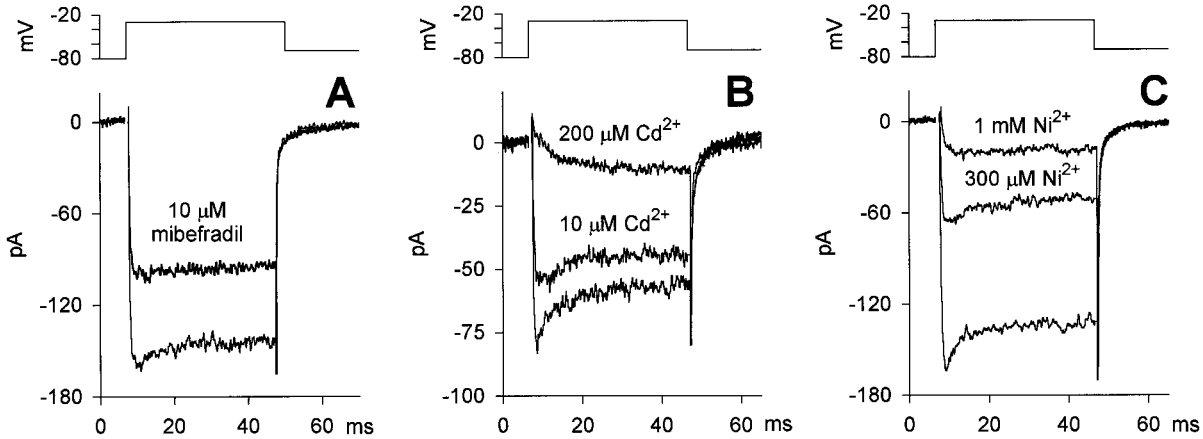

FIGURE 7 Effect of mibefradil (*A*), Cd^{2+} (*B*), and Ni^{2+} (*C*) on the peak and the plateau components of the Ca^{2+} current. The antagonist concentration is indicated above each trace.

$n = 22$; 22 cells); $\tau_{R1} = 0.18 \pm 0.03$ ms (range: 0.08–0.33 ms; $n = 10$; 10 cells). The difference between the total current and the current recorded in nifedipine gave the waveform of the L-type current (Fig. 5, *A* and *B*, *insets*); τ_{aL}, assessed by fitting the rising phase of the latter current, was 0.35 ± 0.06 ms (range: 0.21–0.56 ms; $n = 6$; 6 cells). The time constant τ_{aR2}, drawn from the fit of the currents lacking the sag component in the presence of nifedipine (Fig. 5 *B*), was 0.68 ± 0.08 ms (range: 0.39–0.90 ms; $n = 6$; 6 cells). The above described procedure is legitimate to calculate τ_{aL} and τ_{aR2}, providing that nifedipine does not affect τ_{aR2}. This condition is indeed satisfied here since, in all experiments, no significant difference was found between the values of τ_{aR2} obtained in 1 μM and in 5 μM nifedipine (data not shown).

The responses with or without the sag component had almost identical deactivation kinetics upon returning to the holding potential; in general, it was not possible to record the inward peak tail currents, probably because they were too fast to be resolved by our experimental arrangement (an example is in the inset of Fig. 5, *A* and *B*). Thus, the deactivation phase $I_d(t)$ of the Ca^{2+} current can only be interpolated by:

$$I_d(t) = A_{dL} \cdot e^{-(t/\tau_{dL})} + A_{dR2} \cdot e^{-(t/\tau_{dR2})} \quad (2)$$

The parameters A_{dL} and τ_{dL} are the amplitude and time constant of the deactivation phase of the L-type current: the fit to these currents gave $A_{dL} = A_{aL}$ and $\tau_{dL} = 0.24 \pm 0.05$ ms (range: 0.20–0.33 ms; $n = 6$; 6 cells). The deactivation phase of the noninactivating R-type current was calculated by the fit of the current in nifedipine (Fig. 5, *A* and *B*). The resulting values were $\tau_{dR2} = 8.5 \pm 0.6$ ms (range: 2.0–14.6 ms; $n = 29$; 29 cells) and $A_{dR2} = -18.0 \pm 2.0$ pA (range: -5 to -40 pA; $n = 29$; 29 cells).

I-V characteristics

To further characterize the three channel types it is necessary to determine their voltage dependence. Given the long recovery time from inactivation (Fig. 4), the interpulse duration of the I-V protocols was kept longer than 1 s.

Fig. 8 *A* shows the voltage dependence of the Ca^{2+} current waveform in a typical cell. A peak superimposed on the plateau became appreciable at -40 mV (which is the activation threshold of the R-type channel generating the sag waveform), reaching a maximal value at -30 mV. The peak was progressively reduced by larger depolarizations, and became undetectable for voltages ≥ 0 mV. The plateau component, generated by the noninactivating R-type channel and the L-type channel, was appreciable at -60 mV, peaked at -20 mV, and had a reversal potential (V_{rev}) of $\sim +50$ mV. The I-V relationships for the peak and plateau components are illustrated in panel *B* (*open diamonds* and *filled circles*, respectively). The normalized average I-V of the peak (*open diamonds*) and plateau (*filled circles*) components are shown in Fig. 9 *A*; since no significant changes were found in the I-V relationships recorded using different pipette $[Ca^{2+}]$, the data for these I-V relationships were averaged together. The I-V of the plateau component exhibited a V_{rev} of $+40$ mV (Fig. 9 *A*, *filled circles*), smaller than would be expected from the Nernstian reversal potential for Ca^{2+} (>200 mV). However, the current never reversed for depolarizations up to $+60$ mV when $[Cs^+]_i$ was substituted with an equiosmolar concentration of the large impermeant cation NMG^+ (Fig. 9 *A*, *open triangles*). Furthermore, as shown in Fig. 9 *B*, the size of the outward current was progressively reduced as the Ca^{2+} current declined during the run-down (see the "run-down" section and Fig. 2, *B* and *C*), indicating that most of the Cs^+ current flowed through the Ca^{2+} channel itself.

The I-V relationships of the two channels generating the plateau component were isolated using a voltage ramp of appropriate steepness (0.56 mV/ms), so that the R-type channel generating the peak was inactivated and did not contaminate the plateau amplitude. The I-V relationship of the noninactivating R-type channel (R2) was obtained in the presence of 5 μM nifedipine; subtracting the R2-type channel I-V from the total current I-V (i.e., the current recorded in the absence of nifedipine), gave the I-V of the L-type current (Fig. 9 *C*). Interestingly, when normalized to the same maximal current amplitude (which was attained at -20 mV for both currents; Fig. 9 *A*), the R2-type and the L-type channel I-V values were undistinguishable up to ~ 0 mV; above this voltage, the L-type current I-V was always below that of the R2-type. In fact, at more depolarized voltages, the latter channel carried all the outward current. Accordingly, the normalized L-type current could not be distinguished from the normalized average I-V relationship recorded when the internal Cs^+ was substituted with NMG^+ (Fig. 9 *A*).

Run-down

The run-down occurred in all cells after several minutes of whole-cell recording and was accelerated by the duration of channel activation, as illustrated in the experiment of Fig. 2 *C*, where the Ca^{2+} current was probed a few times over a long recording. Indeed, the run-down ensued later than it did during stimulation at higher frequency (Fig. 2 *B*). It has been shown that the run-down of L-type cardiac Ca^{2+} currents can be prevented by calpastatin, an inhibitor of the cytoplasmic Ca^{2+}-dependent proteases (Schmid et al., 1995; Seydl et al., 1995; Kameyama et al., 1997, 1998). To verify whether a similar mechanism operates in semicircular canal hair cells, 2 U/ml of calpastatin were incorporated into the pipette solution. Calpastatin completely prevented the run-down, even in cells where the initial response was not particularly large, and despite the heavily sustained and

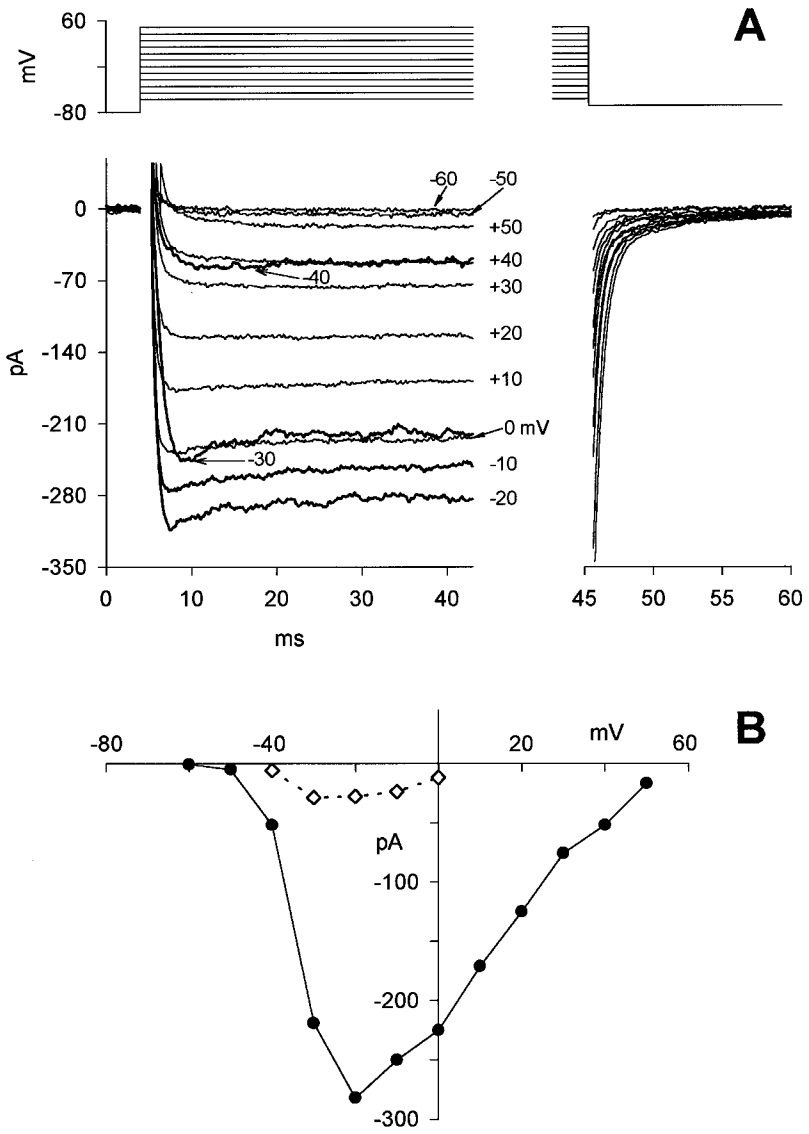

FIGURE 8 I-V characteristics of the current exhibiting the sag. (*A; left panel*) Ca^{2+} currents were elicited by depolarizing voltage pulses from −60 mV to +50 mV in 10-mV increments, from a potential of −80 mV; *right panel*, deactivation kinetics upon returning to the holding potential (−70 mV). (*B*) Steady-state (*filled circles*) and peak (*open diamonds*) current amplitudes from each trace of the cell shown in *A* are plotted against the test potential.

repetitive activation of the current. Indeed, the size and waveform of the current families illustrated in Fig. 10 remained virtually unchanged, although the cell was stimulated with three sequences of 20 depolarizing steps, delivered at 15-s intervals, and lasting 40 ms (*B* and *D*) or 280 ms (*C*; the whole-cell recording time was ~20 min).

Run-up

Surprisingly, in some cells the amplitude of the plateau component progressively increased upon repeating the depolarizing step (before the onset of the run-down; Fig. 11), even doubling in size when compared to the beginning of the recording. This phenomenon has been described in other systems (see, for example, Mironov and Lux, 1991) and it is commonly referred to as current "run-up." The run-up observed here cannot be ascribed to the facilitation sustained by a kinase-induced phosphorylation of a site exposed by channel opening (Dolphin, 1996). Indeed, a 300-ms conditioning depolarization to +40 mV failed to induce any increase in either peak or steady-state amplitude of the current elicited by a test depolarization to −20 mV (data not shown). The run-up of the plateau component was never accompanied by run-up of the sag component: this means that the inactivating R-type channel did not manifest run-up, but only run-down. Furthermore, the run-down kinetics of the latter channel was always independent of the run-up. To determine whether the run-up of the plateau component was generated by a progressive increase in either the L-type current or the noninactivating R-type current (or by both events), the effect of nifedipine during the run-up occurrence was measured. Indeed, the noninactivating R-type current did not appreciably change in amplitude, although the L-type current almost doubled in size (Fig. 11 *C*).

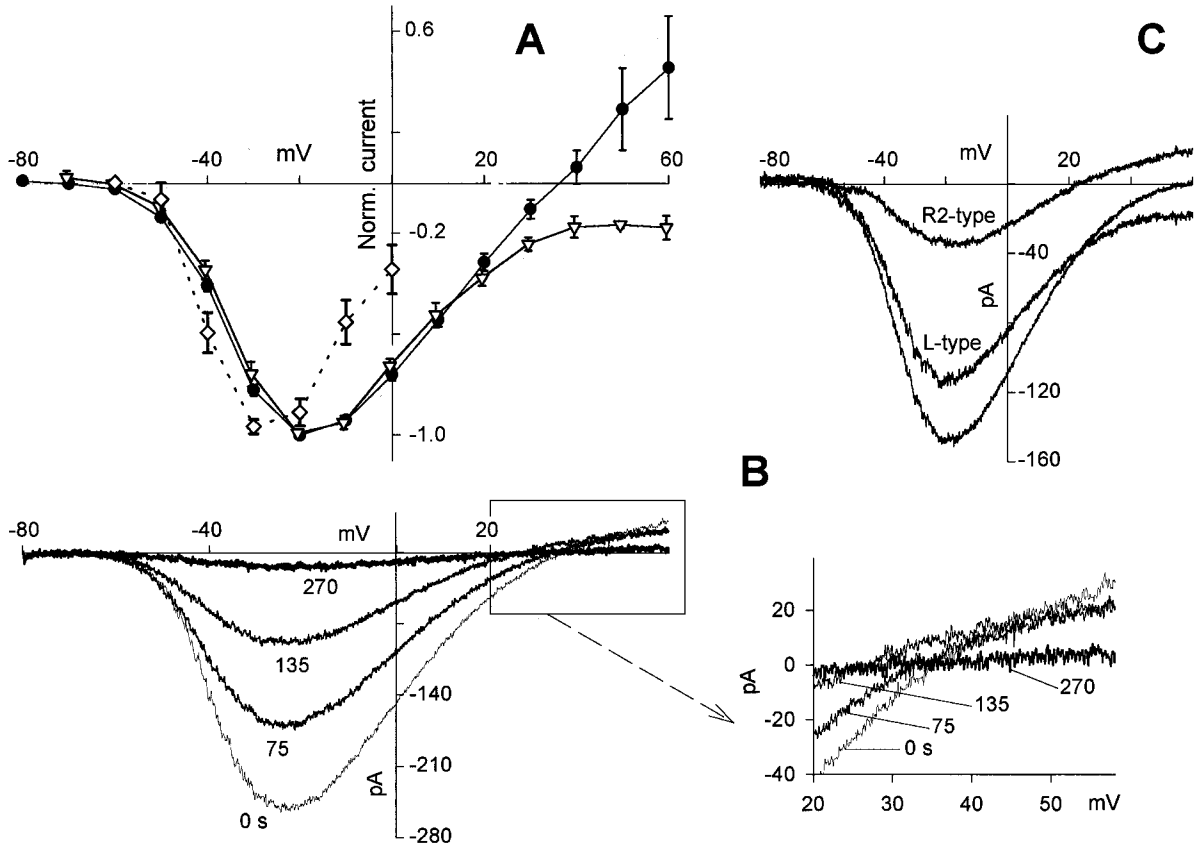

FIGURE 9 Voltage dependence of the R-type and the L-type currents. Ca^{2+} currents in the presence of intracellular Cs^+ or NMG^+ (90 mM). (*A*) Normalized I-V values of the average sag component in Cs^+ (i.e., the inactivating R-type current scaled to the maximal value of A_{R1}, attained at −30 mV, *open diamonds*, 15 cells); the average plateau component in Cs^+ (scaled to the maximal value of the plateau current, attained at −20 mV, *filled circles*, 15 cells); and in NMG^+ (*open triangles*, 7 cells); the R2-type component (*gray noisy trace*) and the L-type component (*gray noisy trace* matching the *open triangles*) of the cell in *C*. In NMG^+, voltages are corrected for the junction potential with respect to Cs^+ (+9 mV). (*B*) I-V relationships in Cs^+, elicited during run-down by voltage ramps of steepness 0.63 mV/ms, from −80 mV to +60 mV, repeated every 15 s. These representative traces were recorded at the beginning of the experiment (0 ms, *thin trace*) and at three subsequent times (75, 135, and 270 s; *thicker traces*); the current responses to the ramp for a voltage interval between +20 and +60 mV (*box*) are enlarged on the right. (*C*) I-V relationships of a cell having a small V_{rev} in response to a ramp of voltage (0.56 mV/ms): I-V of the total current (*unmarked trace*), of the current in the presence of nifedipine (*R2-type trace*) and of the current resulting from the difference between the two latter currents (*L-type trace*).

The magnitude and kinetics with which the run-up developed were independent of the pipette [Ca^{2+}] (ranging from Ca^{2+}-free + 5 mM EGTA to EGTA-free + 0.5 mM Ca^{2+}) and were virtually unchanged when the current was carried by Ba^{2+} instead of Ca^{2+} (data not shown). Generally, when the membrane was depolarized for times ≤40 ms, the current run-up was particularly evident in cells showing large initial currents (Fig. 11 *A*). Even in these cells, if the steps were too long, no run-up was observed, but at most, the L-type current amplitude remained stable for a relatively long time before the run-down onset.

DISCUSSION

It has been previously reported that, in semicircular canal hair cells, the Ca^{2+} currents recorded under whole-cell conditions are carried by a homogeneous population of channels: an L-type channel has been suggested to operate in the frog (Prigioni et al., 1992), whereas a T-type channel has been characterized in the guinea-pig (Rennie and Ashmore, 1991). In contrast with these findings, and according to more recent data (Su et al., 1995; Green et al., 1996; Perin et al., 1998), the present results indicate the existence of a heterogeneous population of three Ca^{2+} channel types in the semicircular canal hair cells. This conclusion was drawn for the following reasons. First of all, the Ca^{2+} current waveform cannot be explained in terms of the opening, and subsequent inactivation, of a single channel population, since this would not account for either the lack of inactivation in some recordings, or the fact that the sag amplitude and its decay time constant never correlate with the plateau current amplitude. This is particularly evident during both run-up and run-down, where the relative amplitudes of the two current components undergo dramatic changes. Arm-

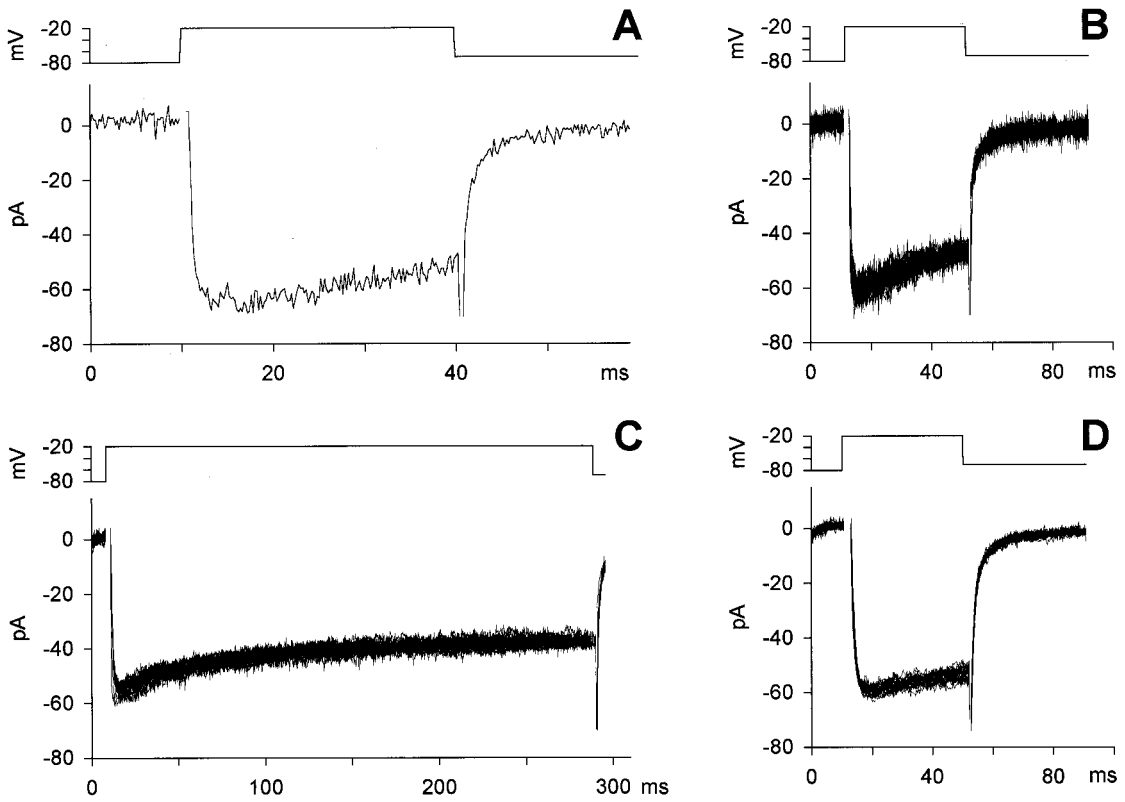

FIGURE 10 Effect of intracellular perfusion of 2 U/ml calpastatin on the current amplitude and waveform. (*A*) Typical Ca^{2+} current elicited by −20 mV depolarization from a potential of −80 mV. (*B–D*) Responses of the same cell to a sequence of 60 depolarizing voltage pulses delivered every 15 s and lasting 40, 280, and 40 ms, respectively.

strong and Roberts (1998) have demonstrated that a sag in the Ca^{2+} current (not present in enzymatically dissociated cells, Hudspeth and Lewis, 1988) disappeared when pipette Cs^+ was replaced by NMG^+. Thus, they suggested that this sag is produced by a Cs^+ current flowing through Ca^{2+}-dependent, voltage-independent S_K channels. In the present study, however, the sag was still present when NMG^+ replaced Cs^+ in the pipette solution, or during the external application of 1 μM apamin, a specific S_K channel blocker (data not shown). Furthermore, the sag amplitude was reduced, and its kinetics slowed down, as $[Ca^{2+}]_o$ decreased (Fig. 3 *A*). It is therefore concluded that the sag component

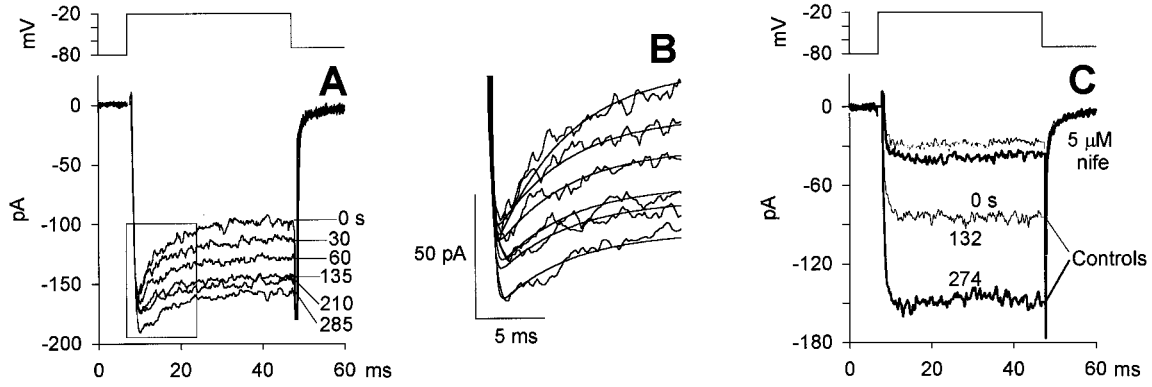

FIGURE 11 Run-up of the plateau component. Current was tested with 40-ms depolarizing voltage steps to −20 mV, repeated every 15 s; (*A*) Cell having a particularly large peak current where the run-down of the peak component and the run-up of the plateau component were evident. Representative traces were recorded at the beginning of the experiment (0 s) and at five subsequent times indicated near each trace. (*B*) Enlargement of the same traces as in *A* (*box*) and fits to Eq. 1 of the data (*smooth lines*). (*C*) Run-up of a cell lacking the sag component and effect of nifedipine on the current recorded at 0 s (*thin black trace*), 132 s (*thick gray trace*), and 274 s (*thick black trace*).

is generated by a Ca^{2+} channel distinct from the channel(s) generating the plateau.

Pharmacological experiments were used next to identify the channel type generating the sag and plateau components. Both components were resistant to ω-conotoxin GVIA (concentration tested: 1, 5, and 10 μM), ω-conotoxin MVIIC (5 μM), and ω-agatoxin IVA (concentration tested: 0.2 and 0.4 μM) and they were sensitive to Ni^{2+} and Cd^{2+} (≥10 μM). The sag component was sensitive to mibefradil (10 μM). These results indicate the absence of an N-type or a P/Q type channel and suggest that the sag could be generated by a T-type channel, with a more positive activation threshold (−40 mV; Fig. 8) than observed in the neuronal T-type channel. However, to our knowledge, no T-type channel has been reported to inactivate in a Ca^{2+}-dependent manner (Tsien et al., 1998); thus it can be concluded that the sag component is generated by either a novel T-type channel or by an inactivating R-type channel. The plateau component was greatly reduced, but not cancelled out, by nifedipine (5 μM), indicating that this component is generated by an L-type and a second, noninactivating, R-type channel. The L-type channel activation threshold (−60 mV, Figs. 8 and 9) is significantly more negative than the neuronal L-type channel, and it does not have any steady-state inactivation at the resting potential (neither do the other two R-type channels). The L-type channel observed here is more selective to Ca^{2+} and has faster activation-deactivation kinetics than the noninactivating R-type channel. Nevertheless, the inward tail current was so fast that it could not be resolved. Therefore, Eq. 2 is most likely incomplete, describing the later deactivation kinetics. The voltage-dependent activation and deactivation kinetics observed here are faster than previously described in the frog (0.2–0.6 ms vs. 3.2–5.2 ms); this is most likely due to the cell isolation procedure, i.e., mechanical versus enzymatic dissociation. This view is supported by the recent findings of Armstrong and Roberts (1998), who clearly demonstrated that the main electrical properties of frog saccular hair cells, i.e., the voltage oscillation in response to injected currents and the time course of both K^+ and Ca^{2+} currents (Hudspeth and Lewis, 1988), are markedly affected by the enzymatic treatment.

Ca^{2+}-dependent inactivation of the R-type channel

The absence of the sag in the Ba^{2+} current elicited by a depolarization indicates that a Ca^{2+}-dependent inactivation process occurs when $[Ca^{2+}]_i$ rises as a consequence of channel opening. In apparent contrast with this view, sag kinetics was never slowed down in Ca^{2+}-free + 5 mM EGTA pipette solution as compared to the kinetics of currents recorded in EGTA-free + 0.5 mM Ca^{2+}. In general, Ca^{2+} current amplitude and kinetics, and the extent and time course of both run-up and run-down, were not correlated to the Ca^{2+} and EGTA concentrations used. However, EGTA is far too slow a chelator and does not in any way affect spatial distribution and temporal changes in $[Ca^{2+}]_i$ near an open channel during the Ca^{2+} inflow (Stern, 1992). Moreover, Ca^{2+}-dependent inactivation would predict that τ_{iR1} is progressively reduced during the run-up, but this has not been observed. It is also true that the smaller the current amplitude, the greater τ_{iR1} should be, but this, again, has not been systematically observed: the τ_{iR1} is only slowed down by changing the Ca^{2+} driving force (Fig. 3 *A*). These results suggest that the Ca^{2+} flowing through an open Ca^{2+} channel is sufficient to inactivate the channel itself. If this were the case, the inactivation rate would not be affected by the $[Ca^{2+}]_i$ changes produced by the nearby open channels. As a result, this rate would not correlate with the current amplitude, whereas it would be slowed down upon reduction of the Ca^{2+} driving force (as shown in Fig. 3 *A*). An inactivation process that is highly sensitive to local $[Ca^{2+}]_i$ would also be indirectly voltage-dependent, because local $[Ca^{2+}]_i$ depends linearly on the Ca^{2+} influx, i.e., on the single channel current amplitude which is, in turn, voltage-dependent. It can be further hypothesized (valid here) that the inactivation is significantly slower than the current activation and deactivation. If this were the case, the inactivation rate voltage dependence would have to correlate with the voltage dependence of the sag current (Sherman et al., 1990), as was indeed found (Fig. 8 *A*).

The faster recovery of the sag component occurring at −120 mV when compared to −70 mV in the double-pulse protocol experiments (Fig. 4 *D*) can be explained by an acceleration of the Ca^{2+} extrusion, possibly via a Na^+/Ca^{2+} exchanger. Indeed, the plasma membrane Ca^{2+} pump is probably electroneutral (Laüger, 1992) and is not expected to be voltage-dependent, whereas the Na^+/Ca^{2+} exchanger is accelerated by the hyperpolarization, since it imports one net positive charge per exchange cycle (Laüger, 1992; Rispoli et al., 1995). Furthermore, the existence of a Ca^{2+}-ATPase has been found at the level of hair cell stereocilia (Gioglio et al., 1998; Yamoah et al., 1998), but not at the level of the basolateral membrane, which has been suggested as a possible site for a Na^+/Ca^{2+} exchanger (Chabbert et al., 1995; Gioglio et al., 1998).

The size of the current increase observed upon substituting Ca^{2+} with Ba^{2+} was smaller in the cells lacking the sag component than in those exhibiting the sag (compare Fig. 5 *C* and the corresponding inset on the right with Fig. 5 *D* and the inset on the right). This can be explained by the greater permeability to Ba^{2+} of the inactivating R-type channel and/or by assuming that the inactivation process begins before the current has fully developed.

Run-down

In the absence of the protease inhibitor calpastatin, a Ca^{2+} current run-down eventually developed in all recordings lasting >5–7 min. The run-down affected all the observed

channel types, although the R-type channel generating the sag component ran down faster than the other two (Fig. 2 *B*). All channel types, however, are the target of the same protease, since calpastatin prevented the run-down (Fig. 10). A considerable wash-out of one or more of the endogenous protease inhibitors through the patch pipette is likely, since the current run-down depended on the whole-cell recording time and access resistance. However, since the proteases responsible for this phenomenon are known to be activated by Ca^{2+} (and by Ba^{2+}, see Results), it is possible that the nonphysiological activation of the Ca^{2+} channels in the repetitive stimulation experiments eventually caused a buildup of $[Ca^{2+}]_i$ and to such an extent as to stimulate proteolysis. Indeed, the run-down was accelerated by pipette $[Ca^{2+}] > 1$ mM, which overloaded the cell's Ca^{2+} extrusion mechanism and endogenous buffering capacity. Additional evidence for a Ca^{2+}-dependent protease is given by the delayed run-down observed when the duration of channel activation is decreased (i.e., decreasing the Ca^{2+} influx; Fig. 2 *C*) as compared to the run-down observed during repeated stimulation at higher frequencies (Fig. 2 *B*).

The waveform of each trace during run-down could be interpolated by fitting the data to Eq. 1 at the beginning of the experiment, and by progressively reducing amplitudes A_L, A_{R1}, and A_{R2} as the current size decreased (Fig. 2, *B* and *C*). This indicates that the run-down is simply generated by the progressive reduction in the number of channels, although their activation, inactivation, and deactivation kinetics are preserved.

From a physiological point of view, the proteases could be implicated in continuous channel turn-over, i.e., the removal of old proteins and their replacements with those freshly synthesized. The proteases might also play an important role as safety devices, by preventing lethal Ca^{2+} entry.

Run-up

The L-type channels may produce large and sustained currents, and could, therefore, cause large Ca^{2+} changes throughout the cytoplasm, not just in the local region close to the plasma membrane. Therefore, one would expect that strict control be exerted over the Ca^{2+} transport generated by these channels, through a regulatory mechanism the sign of which is the run-up described in the Results. Unfortunately, the occurrence of the run-up phenomenon prevented the acquisition of either a large number of short current traces of the same amplitude or long steady-state recordings, thus preventing the evaluation of single channel parameters through noise analysis (either nonstationary or stationary). However, as was the case for run-down, the waveform of each trace during the run-up could be interpolated by Eq. 1 at the beginning of the experiment, this time by progressively increasing A_L and decreasing (or leaving constant) A_{R1} and A_{R2}, as the current size increased (without changing any activation, inactivation, or deactivation time constants; Fig. 11 *B*). This suggests that the run-up is instead generated by a progressive increase in the number of channels (all having similar properties) opened by repetitive depolarization. Thus, there must be a population of channels that cannot be activated by the initial depolarization and which become progressively available in time. If the run-up is a mechanism by which the cell controls $[Ca^{2+}]_i$ and modulates transmitter secretion, one would expect this mechanism to be Ca^{2+}-dependent; indeed, this is the simplest feedback permitting measurement of the number of activated channels, in order to determine whether more open channels are needed. As pointed out in the Results, no differences were found in the extent and timing of run-up, whether the patch pipette contained 0.5 mM Ca^{2+} or 5 mM EGTA. These solutions did not affect the $[Ca^{2+}]_i$ either in the vicinity of the plasma membrane or farther away (Stern, 1992). Nevertheless, if run-up were triggered by a Ca^{2+}-dependent mechanism, the mechanism should be Ba^{2+}-dependent as well, since the run-up was still present when the current was carried by Ba^{2+}.

Possible role and regulation of three Ca^{2+} channels in the hair cells

One or more of the three channels could be located at the apical receptor pole rather than at the basolateral pole, and could therefore generate adaptation of the transduction process. However, if all Ca^{2+} channel types were located at the basolateral membrane, they could be implicated in synaptic transmission. There are indeed reports implicating the R-type channel in synaptic transmission (see, for example, Wu et al., 1998); therefore the two R-type channels—one providing a sustained current, the other a transient current—could trigger synaptic transmission. If this is the case, the inactivating R-type channel may be functionally important in producing fast (synchronous) transmitter release in response to short, strong stimuli by boosting Ca^{2+} entry to quickly elicit synaptic transmission while, at the same time, preventing too large Ca^{2+} influx, which could be metabolically costly or even lethal to the cell. However, in the presence of a prolonged mechanical stimulus, channel inactivation would produce a reduction in the rate of transmitter release, and in turn the progressive decrease in mEPSP frequency. Indeed, such a decrease has been detected in the excitatory phase of the mEPSP response (recorded from single fibers of the posterior nerve in the intact frog labyrinth). The decrease began to appear at accelerations of $40°/s^2$ and increased as the stimulus intensity was increased up to $87°/s^2$ (Rossi et al., 1989).

The noninactivating R-type channels may instead sustain the ongoing spontaneous receptor activity that could also be mediated by the L-type channel. Indeed, the L-type channel can carry large, sustained Ca^{2+} current, it is highly Ca^{2+}-selective, and is regulated by an intracellular mechanism

that may be important for the response to rather weak, prolonged stimuli. Since the L-type channel may provide controlled Ca^{2+} uptake, it could also play an important role in replenishing the intracellular stores. The Ca^{2+} influx provided by the three channels may also activate the Ca^{2+}-dependent K^+ current, which resets the system by repolarizing the cell.

Many thanks to Prof. Oscar Sacchi, Prof. Emilio Carbone, Dr. Eric Ertel, and Dr. Francesca Noceti for very useful discussions and for reading the manuscript. Many thanks also to Dr. Andrea Moriondo for participating in some experiments.

This work was supported by grants from the Ministero per l'Università e la Ricerca Scientifica e Tecnologica (MURST), Roma, and from the Istituto Nazionale per la Fisica della Materia (INFM), CADY project, Genova, Italy.

REFERENCES

Armstrong, C. E., and W. M. Roberts. 1998. Electrical properties of frog saccular hair cells: distortion by enzymatic dissociation. *J. Neurosci.* 18:2962–2973.

Block, B. M., and S. W. Jones. 1997. Delayed rectifier current of bullfrog sympathetic neurons: ion-ion competition, asymmetrical block and effects of ions on gating. *J. Physiol. (Lond.).* 499:403–416.

Carbone, E., and H. D. Lux. 1984. A low voltage-activated, fully inactivating Ca channel in vertebrate sensory neurones. *Nature.* 310:501–502.

Chabbert, C., Y. Canitrot, A. Sans, and J. Lehouelleur. 1995. Calcium homeostasis in guinea pig type-I vestibular hair cell: possible involvement of an Na^+-Ca^{2+} exchanger. *Hear. Res.* 89:101–108.

Dolphin, A. C. 1996. Facilitation of Ca^{2+} current in excitable cells. *Trends Neurosci.* 19:35–43.

Dunlap, K., J. L. Luebke, and T. J. Turner. 1995. Exocytotic Ca^{2+} channels in mammalian central neurons. *Trends Neurosci.* 18:89–98.

Emanuel, K., U. Mackiewicz, B. Pytkowski, and B. Lewartowski. 1998. Effects of mibefradil, a blocker of T-type Ca^{2+} channels, in single myocytes and intact muscle of guinea-pig heart. *J. Physiol. Pharmacol.* 49:577–590.

Fuchs, P. A., and M. G. Evans. 1990. Potassium currents in hair cells isolated from the cochlea of the chick. *J. Physiol. (Lond.).* 429:529–551.

Fuchs, P. A., M. G. Evans, and B. W. Murrows. 1990. Calcium currents in hair cells isolated from the cochlea of the chick. *J. Physiol. (Lond.).* 429:553–568.

Gioglio, L., G. Russo, W. Marcotti, and I. Prigioni. 1998. Localization of Ca-ATPase in frog crista ampullaris. *Neuroreport.* 9:1309–1312.

Green, G. E., K. M. Khan, D. W. Beisel, M. J. Drescher, J. S. Hatfield, and D. G. Drescher. 1996. Calcium channel subunits in the mouse cochlea. *J. Neurochem.* 67:37–45.

Guth, P. S., C. D. Fermin, M. Pantoja, R. Edwards, and C. Norris. 1994. Hair cells of different shapes and their placement along the frog crista ampullaris. *Hear. Res.* 73:109–115.

Hamill, O. P., A. Marty, E. Neher, B. Sakmann, and F. J. Sigworth. 1981. Improved patch-clamp techniques for high-resolution current recording from cells and cell-free membrane patches. *Pflügers Arch.* 391:85–100.

Housley, G. D., C. H. Norris, and P. S. Guth. 1989. Electrophysiological properties and morphology of hair cells isolated from the semicircular canal of the frog. *Hear. Res.* 38:259–276.

Hudspeth, A. J., and P. G. Gillespie. 1994. Pulling springs to tune transduction: adaptation by hair cells. *Neuron.* 12:1–9.

Hudspeth, A. J., and R. S. Lewis. 1988. Kinetic analysis of voltage- and ion-dependent conductances in saccular hair cells of the bull-frog, *Rana catesbeiana*. *J. Physiol. (Lond.).* 400:237–274.

Huguenard, J. R. 1998. Low-voltage-activated (T-type) calcium-channel genes identified. *Trends Neurosci.* 21:451–452.

Kameyama, M., A. Kameyama, E. Takano, and M. Maki. 1998. Run-down of the cardiac L-type Ca^{2+} channel: partial restoration of channel activity in cell-free patches by calpastatin. *Pflügers Arch.* 435:344–349.

Kameyama, A., K. Yazawa, M. Kaibara, K. Ozono, and M. Kameyama. 1997. Run-down of the cardiac Ca^{2+} channel: characterization and restoration of channel activity by cytoplasmic factors. *Pflügers Arch.* 433:547–556.

Lang, D. G., and M. J. Correia. 1989. Studies of solitary semicircular canal hair cells in the adult pigeon. II. Voltage-dependent ionic conductances. *J. Neurophysiol.* 62:935–945.

Laüger, P. 1992. Electrogenic ion pumps. Sinauer Associates, Sunderland, MA.

Masetto, S., G. Russo, and I. Prigioni. 1994. Differential expression of potassium currents by hair cells in thin slices of frog crista ampullaris. *J. Neurophysiol.* 72:443–455.

McCleskey, E. W. 1994. Calcium channels: cellular roles and molecular mechanisms. *Curr. Opin. Neurobiol.* 4:304–312.

Mironov, S. L., and H. D. Lux. 1991. Calmodulin antagonists and protein phosphatase inhibitor okadaic acid fasten the 'run-up' of high-voltage activated calcium current in rat hippocampal neurones. *Neurosci. Lett.* 133:175–178.

Norris, C. H., A. J. Ricci, G. D. Housley, and P. S. Guth. 1992. The inactivating potassium currents of hair cells isolated from the crista ampullaris of the frog. *J. Neurophysiol.* 68:1642–1653.

Ohmori, H. 1984. Studies of ionic currents in the isolated vestibular hair cell of the chick. *J. Physiol. (Lond.).* 350:561–581.

Perin, P., G. B. Athas, M. M. Garcia, S. Masetto, P. Valli, P. S. Holt, and P. S. Guth. 1998. Voltage-operated calcium channel expression by frog vestibular hair cells. ARO Midwinter Research Meeting, St. Petersburg, FL, Abstr. 577.

Prigioni, I., S. Masetto, G. Russo, and V. Taglietti. 1992. Calcium currents in solitary hair cells isolated from frog crista ampullaris. *J. Vest. Res.* 2:31–39.

Randall, A. D., and R. W. Tsien. 1997. Contrasting biophysical and pharmacological properties of T-type and R-type calcium channels. *Neuropharmacology.* 36:879–893.

Rennie, K. J., and J. F. Ashmore. 1991. Ionic currents in isolated vestibular hair cells from the guinea-pig crista ampullaris. *Hear. Res.* 51:279–291.

Rispoli, G., A. Navangione, and V. Vellani. 1995. Transport of K^+ by photoreceptor Na^+/Ca^{2+}, K^+ exchanger in isolated rods of lizard retina. *Biophys. J.* 69:74–83.

Rossi, M. L., C. Bonifazzi, M. Martini, and R. Fesce. 1989. Static and dynamic properties of synaptic transmission at the cyto-neural junction of frog labyrinth posterior canal. *J. Gen. Physiol.* 94:303–327.

Rossi, M. L., M. Martini, B. Pelucchi, and R. Fesce. 1994. Quantal nature of synaptic transmission at the cytoneural junction in the frog labyrinth. *J. Physiol. (Lond.).* 478:17–35.

Schmid, R., K. Seydl, W. Baumgartner, K. Groschner, and C. Romanin. 1995. Trypsin increases availability and open probability of cardiac L-type Ca^{2+} channels without affecting inactivation induced by Ca^{2+}. *Biophys. J.* 69:1847–1857.

Seydl, K., J. O. Karlsson, A. Dominik, H. Gruber, and C. Romanin. 1995. Action of calpastatin in prevention of cardiac L-type Ca^{2+} channel run-down cannot be mimicked by synthetic calpain inhibitors. *Pflügers Arch.* 429:503–510.

Sherman, A., J. Keizer, and J. Rinzel. 1990. Domain model for Ca^{2+}-inactivation of Ca^{2+} channels at low channel density. *Biophys. J.* 58: 985–995.

Steinacker, A., J. Monterrubio, R. Perez, A. F. Mensinger, and A. Marin. 1997. Electrophysiology and pharmacology of outward potassium currents in semicircular canal hair cells of toadfish, *Opsanus tau*. *Hear. Res.* 109:11–20.

Stern, M. D. 1992. Buffering of calcium in the vicinity of a channel pore. *Cell Calcium.* 13:183–192.

Su, Z. L., S. C. Jiang, R. Gu, and W. P. Yang. 1995. Two types of calcium channels in bullfrog saccular hair cells. *Hear. Res.* 87:62–68.

Tsien, R. W., J. P. Clozel, and J. Nargeot. 1998. Low-voltage activated T-type calcium channels. Adis International LTD, Tottenhall, Chester, UK.

Wu, L. G., J. G. Borst, and B. Sakmann. 1998. R-type Ca^{2+} currents evoke transmitter release at a rat central synapse. *Proc. Natl. Acad. Sci. USA.* 95:4720–4725.

Yamoah, E. N., E. A. Lumpkin, R. A. Dumont, P. J. S. Smith, A. J. Hudspeth, and P. G. Gillespie. 1998. Plasma membrane Ca^{2+}-ATPase extrudes Ca^{2+} from hair cell stereocilia. *J. Neurosci.* 18:610–624.

Zidanic, M., and P. A. Fuchs. 1995. Kinetic analysis of barium currents in chick cochlear hair cells. *Biophys. J.* 68:1323–1336.